analytical chemistry

pubs.acs.org/ac Article

$AgInSe_2$-Sensitized ZnO Nanoflower Wide-Spectrum Response Photoelectrochemical/Visual Sensing Platform via Au@Nanorod-Anchored CeO_2 Octahedron Regulated Signal

Shaopeng Wang,[#] Fangfang Wang,[#] Cuiping Fu,[#] Yina Sun, Jinge Zhao, Na Li, Yunqing Liu,* Shenguang Ge,* and Jinghua Yu

Cite This: https://dx.doi.org/10.1021/acs.analchem.0c00231 Read Online

ACCESS | Metrics & More | Article Recommendations | Supporting Information

ABSTRACT: Herein an ultrasensitive photoelectrochemical (PEC)/visual biosensor coupled with a multiple signal amplification strategy was proposed for the detection of nucleic acids. The initial signal amplification was achieved via ternary $AgInSe_2$ quantum dot (QD)-sensitized ZnO nanoflowers (ZnO NFs) to form an excellent photoelectric layer. A gold-modified nanorod-anchored CeO_2 (Au@NR−CeO_2) octahedron was introduced as a multifunctional signal regulator via the formation of triple helix molecules. The Au@NR−CeO_2 octahedron could not only quench the photocurrent signal due to the competitive capture of photon energy and electron donors with the photoelectric layer but could also act like a peroxidase to catalyze the formation of mimetic enzymatic catalytic precipitation (MECP) on the surface of the photoelectric layer. Furthermore, the steric hindrance effect from the Au@NR−CeO_2 octahedron further reduced the output of the photocurrent signal. After incubation with t-DNA, the triple helix conformation was disassembled and the Au@NR−CeO_2 octahedron was released from the electrode surface, leading to the significant increase of photocurrent signal. Meanwhile, the released Au@NR−CeO_2 octahedron could flow into the colorimetric area of the lab-on-paper device to catalyze the occurrence of the color reaction, achieving a visual detection for t-DNA. On the basis of the multiple signal amplification strategy, t-DNA was detected specifically with a lower limit of detection of 0.28 fM and a wider linear range from 0.5 fM to 50 nM. The proposed method has the potential utility to detect a variety of nucleic acids and biomarkers.

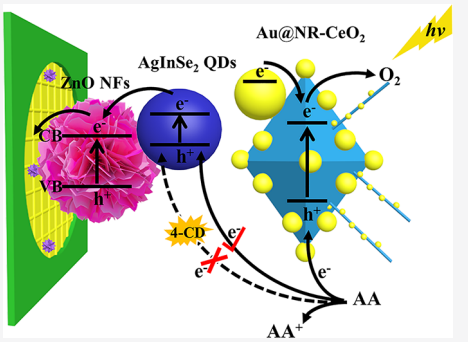

Photoelectrochemical (PEC) detection is a vigorously developed analytical method, based on the PEC process and chemical or biological probing recognition.[1−4] It has shown broad application potential in life analysis and cancer early warning due to the higher sensitivity, low-cost instruments, and inherent miniaturization.[5−9] In the construction of PEC biosensors, the choice of superior photoelectric materials and the design of signal amplification strategies are crucial and prerequisite for improving photocurrent signals.[10,11] Lab-on-paper devices have attracted vast attention in the construction of biosensors due to low cost, simple production, double-sided processing, adjustable hydrophilicity and hydrophobicity, and the realization of visual detection. ZnO is widely used as a photoactive material on account of its admirable chemical stability and acceptable photoelectric properties.[12−14] However, the inherent wide band gap of ZnO has limited the photocurrent conversion efficiency.[15] To further enhance the photocurrent intensity, some small band gap semiconductor materials were chosen to sensitize ZnO, such as CdS quantum dots (QDs), CdTe QDs, and PbS QDs, which could broaden the absorption range of light and accelerate the electron−hole separation efficiency.[16−18] Nevertheless, Cd-containing and Pb-containing QDs are toxic, hindering their further development in biosensing.[19,20] So exploring a low toxicity QD is crucial and necessary for the future construction of the biosensors.

In recent years, ternary I−III−VI_2 QDs have received increasing interest owing to the low toxicity and similar outstanding photoelectric properties compared with binary II−VI or IV−VI QDs containing highly toxic elements.[21−23] It has become the best alternative to binary QDs and exhibited merits in solar cells and biomedical imaging.[24] However, as far as we know, it is rarely applied in the construction of PEC biosensors. $AgInSe_2$ is a typical ternary group I−III−VI_2 QD with a band gap of 1.24 eV, which is suitable as a promising photosensitizer and light harvester for PEC biosensors owing to its relatively large light absorption range and satisfactory band gap.[25,26] Herein we synthesized glutathione-stable

Received: January 17, 2020
Accepted: May 4, 2020
Published: May 4, 2020

Scheme 1. Fabrication Process of the PEC/Visual Biosensor for Detection of t-DNA

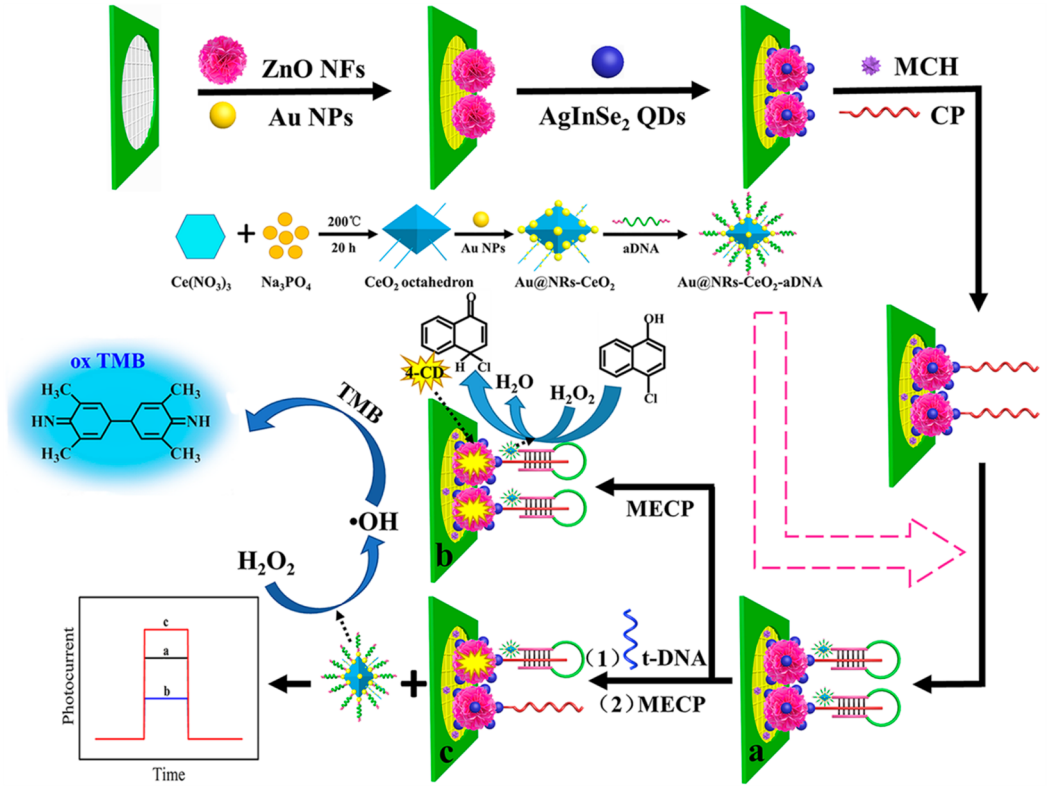

$AgInSe_2$ QDs (GHS-$AgInSe_2$ QDs) in the aqueous phase, which could effectively promote electron transfer from the $AgInSe_2$ QDs to the conduction band of ZnO due to the satisfactory energy level matching and multidentate chelating effect of the glutathione stabilizer.

In addition to achieving outstanding initial signal amplification, the design of the efficient quenching effects also plays a key role in increasing sensitivity of the PEC biosensor.[10,27] Up to now, common quenching effects have mainly included steric hindrance, enzymatic reactions, and energy transfer.[28−30] Enzymatic reactions are a method of quenching the photocurrent signal by generating insoluble precipitates on the electrode surface.[31,32] Biocatalytic precipitation based on natural enzymes has also been extensively reported.[33] However, the inherent disadvantages of natural enzymes limit further application in biosensors.[34] It is therefore urgent to develop an enzyme mimic that can not only overcome the problems of low stability but can also catalyze the production of precipitation.[35,36] In the past few years, cerium dioxide (CeO_2) has drawn much attention in optical limiters, photocatalysis, and biosensors due to its favorable electrical, optical, and peroxidase-like properties.[37−39] On the other hand, for energy transfer, alot of previous work has proved that energy transfer between gold nanoparticles (Au NPs) and QDs can significantly quench photocurrent signals.[40,41] Meanwhile, Au NPs also have excellent electric conductivity and superior electrocatalytic properties toward H_2O_2 reduction.[42] In addition, the surface plasmon resonance (SPR) of Au NPs can accelerate the electron conversion efficiency of semiconductors.[43] Inspired by the superior performance of CeO_2 and Au NPs, we synthesized a Au−CeO_2 nanocomposite and researched applications in the construction of a PEC/visual biosensor.

Herein, a multiple signal amplification PEC/visual biosensor was developed based on ternary $AgInSe_2$ QD-sensitized ZnO nanoflowers (ZnO NFs) and a gold-modified nanorods-anchored CeO_2 (Au@NRs−CeO_2) octahedron as a multifunctional signal regulator for detection of nucleic acids (Scheme 1). The pictures of the lab-on-paper device (Figure S1) and the nucleic acid sequence (Table S1) are shown in Supporting Information. First, ZnO NFs and $AgInSe_2$ QDs were assembled on the gold nanoparticle-modified paper working electrode (Au−PWE) to form the $AgInSe_2$ QDs/ZnO NFs/Au−PWE photoelectric layer, exhibiting strong initial photocurrent signal. Then the Au@NRs−CeO_2 octahedron labeled one end of assistant DNA (Au@NRs−CeO_2−aDNA) and was introduced to hybridize with a capture probe (CP) to form the triple helix molecules. The Au@NRs−CeO_2 octahedron could quench effectively the photocurrent signal because of the competitive capture of photon energy and electron donors with the photoelectric layer, leading to a noticeable photocurrent signal decrement. In the absence of t-DNA, after the electrode was incubated with a mixture of 4-chloro-1-naphthol (4-CN) and H_2O_2, the Au@NRs−CeO_2 octahedron could act as peroxidase to produce a mimetic enzymatic catalytic precipitation (MECP) on the surface of the photoelectric layer, further quenching the photocurrent signal. However, when t-DNA was present, it could hybridize with the loop of Au@NRs−CeO_2−aDNA to disassemble the triple helix molecules, resulting in Au@NRs−CeO_2 octahedron release from the electrode interface and disappearance of the quenching effect, which made the photocurrent signal greatly increase. Meanwhile, the released Au@NRs−CeO_2 octahedron flowed into the colorimetric area of lab-on-paper device and then catalyzed the chromogenic substrate 3,3′,5,5′-tetrame-

https://dx.doi.org/10.1021/acs.analchem.0c00231
Anal. Chem. XXXX, XXX, XXX−XXX

thylbenzidine (TMB) to form the colored product, achieving an intuitive detection of t-DNA.

EXPERIMENTAL SECTION

Synthesis of the Au@NRs−CeO_2 Octahedron. The Au@NRs−CeO_2 octahedron was synthesized as a multifunctional signal regulator for the PEC biosensor according to appropriate modification of previous work.[44] An aliquot of 0.0134 g of $Na_3PO_4{\cdot}12H_2O$ was dissolved in 35 mL of ultrapure water and stirred for 10 min, 5 mL of 0.2 M $Ce(NO_3)_3{\cdot}6H_2O$ was added dropwise to the above solution under stirring, and the mixed solution was transferred to an autoclave and reacted at 200 °C for 20 h. After the reaction was completed, precipitates were obtained via centrifugation and washed several times with ultrapure water and absolute ethanol. Subsequently, the sample was transferred to a muffle furnace at a heating rate of 5 °C/min and calcined at 600 °C for 6 h. The calcined nanorods-anchored CeO_2 (NRs−CeO_2) octahedron was dissolved in 8 mL of 1% BSA aqueous solution and stirred at room temperature for 4 h. The BSA-coated NRs−CeO_2 octahedron was collected through centrifugation again, which was suspended in 5 mL of Au NP solution and stirred for 12 h to fully absorb the Au NPs. Then the product was centrifuged at 10 000 rpm for 10 min and washed with ultrapure water several times to remove the residue. Finally, the precipitates were dried at 60 °C for 12 h to obtain the Au@NRs−CeO_2 octahedron. The reference gold-modified CeO_2 (Au−CeO_2) octahedron was prepared in the absence of Na_3PO_4 by using the same method.

Fabrication of $AgInSe_2$ QDs/ZnO NFs/Au−PWE. The fabrication of Au−PWE was based on our previous work.[45] ZnO NFs (synthesis of ZnO NFs in the Supporting Information) were modified on the Au−PWE with the aid of 4-aminothiophenol (PATP). ZnO NFs were dissolved in 0.1 mM PATP ethanol solution, and the mixture was centrifuged three times. Then the obtained precipitates were dissolved in ethanol and dropped onto the Au−PWE to obtain ZnO NFs/Au−PWE. Next, 15 μL of GHS-$AgInSe_2$ QDs (for the synthesis of GSH-$AgInSe_2$ QDs, see Supporting Information) containing 20 mM *N*-(3-(dimethylamino)propyl)-*N*′-ethylcarbodiimide (EDC) and 10 mM *N*-hydroxysuccinimide (NHS) solution was dropwise added to the electrodes and reacted for 2 h at room temperature. Finally, the obtained electrodes were carefully washed with washing buffer, completing the fabrication of the $AgInSe_2$ QDs/ZnO NFs/Au−PWE electrodes.

Fabrication of the PEC/Visual Biosensor and PEC Measurement. First, the electrodes were incubated with 10 μL of 1 μM CP at room temperature for 12 h. To eliminate nonspecific adsorption, 10 μL of 6-mercapto-1-hexanol (MCH) was added to the modified electrodes for 30 min. After that, 30 μL of Au@NRs−CeO_2−aDNA was introduced into the electrodes by forming the triple helix molecules. Next, the obtained electrodes were incubated with 10 mM 4-CN solution containing 1 mM H_2O_2 for 30 min in the absence and presence of t-DNA at different concentrations, respectively. Meanwhile, 20 μL of 20 mM TMB and 20 μL of 0.5 M H_2O_2 were preloaded on the colorimetric area of the lab-on-paper device. Subsequently, 40 μL of PBS solution (pH 7.4) containing AA (0.1 M) was dropped into the working area of the lab-on-paper device. Finally, the electrochemical measurements were carried out by immobilizing and connecting the constructed biosensor to an electrochemical workstation.

RESULTS AND DISCUSSION

Characterization of Photoelectric Layer Materials. The choices of electrode materials and photoelectric layer material play a crucial role in PEC biosensors. Herein a lab-on-paper device was chosen as the platform for the biosensor. Figure 1A,B shows the scanning electron microscope (SEM)

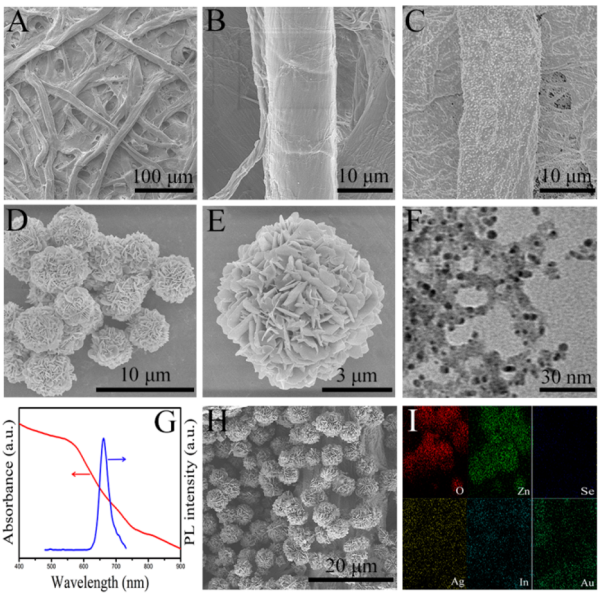

Figure 1. SEM images of (A, B) bare paper cellulose of the PWE at different magnifications. (C) Au−PWE and (D, E) SEM images of ZnO NFs at different magnifications. (F) TEM image of $AgInSe_2$ QDs. (G) UV−vis absorption spectrum and PL spectrum of $AgInSe_2$ QDs. SEM image of (H) $AgInSe_2$ QDs/ZnO NFs/Au−PWE with corresponding element mapping of (I) O, Zn, Se, Ag, In, and Au, respectively.

images of the bare paper electrode at different magnifications, revealing that the bare paper chip was composed of criss-crossed cellulose fiber. After Au NPs were grown in situ on the paper electrode, a continuous, uniform, and thin layer of Au seeds was present on the surface of the paper fiber (Figure 1C), which was advantageous for improving the electrical conductivity of the paper electrode and the load of the photoelectric materials. To obtain the ideal initial photocurrent signal, ZnO nanomaterial was synthesized by a simple hydrothermal method. As illustrated in Figure 1D and E, the morphology of ZnO was nanoflowers of uniform size, and it could be observed clearly that ZnO NFs were assembled from a large number of nanosheets with a layered structure, which increased greatly the specific surface area of the ZnO. To further broaden the absorption range of light and promote the transfer of photogenerated electrons, ternary $AgInSe_2$ QDs were employed to sensitize the ZnO NFs. Figure 1F,G shows the TEM images and UV−vis absorption and photoluminescence (PL) spectra of the prepared $AgInSe_2$ QDs, respectively. As shown in Figure 1F, the $AgInSe_2$ QDs have an average diameter of about 3.2 nm and possess good dispersity due to being coated with a large amount of GHS. In the process of synthesizing $AgInSe_2$ QDs, suitable stabilizers are essential to prevent nanoparticle aggregation. UV−vis

https://dx.doi.org/10.1021/acs.analchem.0c00231
Anal. Chem. XXXX, XXX, XXX−XXX

absorption and PL spectra were used to characterize the optical property of the $AgInSe_2$ QDs. $AgInSe_2$QDs have a broad absorption spectral range from 400 to 900 nm and a distinct exciton peak at 570 nm (Figure 1G), which can absorb light of near-infrared wavelength. The PL emission peak of $AgInSe_2$ QDs is located at 675 nm. Here the photoelectric layer of the PEC biosensor was constructed by sequentially modifying ZnO NFs and $AgInSe_2$ QDs onto the Au−PWE. To clearly demonstrate the successful preparation of the photoelectric layer, the obtained images from SEM and energy-dispersive spectroscopy (EDS) are shown in Figure 1H,I, respectively. As shown in Figure 1H, ZnO NFs were successfully loaded onto the fiber surface and densely grown in the radial direction. After ZnO NFs were modified with $AgInSe_2$ QDs, the surface of ZnO NFs darkened but still retained the original structure due to the small size of $AgInSe_2$ QDs. In addition, Ag, In, and Se were uniformly distributed in the ZnO NFs (Figure 1I). The presence of Au further proved that the Au NPs were successfully grown on the paper electrode.

Characterization of the Au@NRs−CeO_2 Octahedron. In this work, the synthesis of the Au@NRs−CeO_2 octahedron is critical due to its role as a multifunctional signal regulator. Figure 2A shows the SEM image of the prepared CeO_2; the particle morphology observed was octahedral in structure and was anchored by nanorods, which can provide more specific surface area for the loading of Au NPs. To achieve efficient catalytic and quenching properties, Au NPs were modified onto the surface of CeO_2 to form the Au@NRs−CeO_2 octahedron. Figure 2B shows that the CeO_2 surface was covered by many tiny spots with homogeneous structure unevenly distributed. Meanwhile, the UV−vis absorption spectrum was utilized to further demonstrate the formation of the Au@NRs−CeO_2 octahedron. From Figure 2C, the Au@NRs−CeO_2 octahedron revealed a typical absorption range of 500−600 nm in the visible light region, which is the surface plasmon energy band characteristic of Au NPs. It is worth mentioning that the concentration of Na_3PO_4 can affect the amount of nanorods formed. The gold-modified CeO_2 (Au−CeO_2) octahedron just exhibited a regular octahedron without nanorods in the absence Na_3PO_4 (Figure S2). As shown in Figure 2D, the application of the Au@NRs−CeO_2 octahedron showed a photocurrent signal lower than that of the Au−CeO_2 octahedron, which demonstrated that the Au@NRs−CeO_2 octahedron possesses more efficient quenching performance due to its high specific surface area.

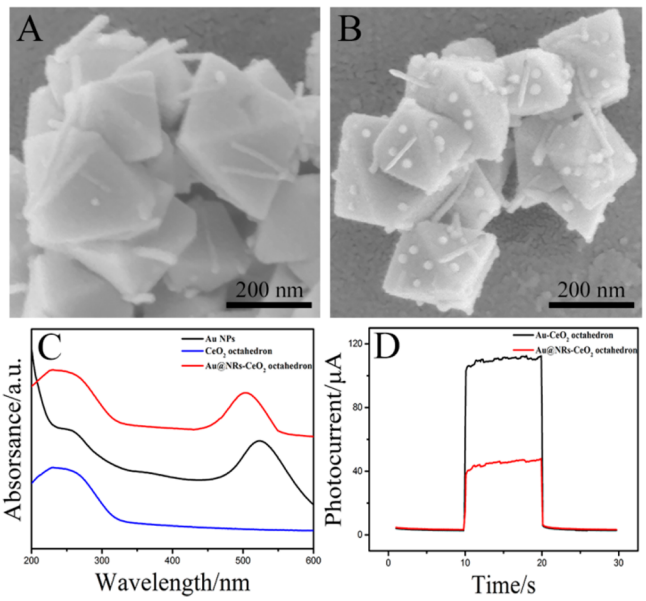

Figure 2. SEM images of the (A) NRs−CeO_2 octahedron and (B) Au@NRs−CeO_2 octahedron. (C) UV−vis absorption spectra of Au NPs, CeO_2 octahedron, and Au@NRs−CeO_2 octahedron. (D) Photocurrent response of the Au−CeO_2 octahedron and Au@NRs−CeO_2 octahedron.

PEC Mechanism of the Biosensor. The multiple signal amplification mechanism of the proposed PEC biosensor is illustrated in Scheme 2. As shown in Scheme 2A, to achieve an excellent initial amplified photocurrent signal, ZnO NFs were sensitized by the ternary $AgInSe_2$ QDs to form a cascade band edge energy level, which could not only improve the utilization of light energy owing to the wide absorption range of $AgInSe_2$ QDs but also promote electron transfer due to the desirable energy level matching between ZnO NFs and $AgInSe_2$ QDs, resulting in an obviously enhanced initial photocurrent signal. For the quenching mechanism, the Au@NRs−CeO_2 octahedron was introduced through forming triple helix molecules, which could act as a multifunctional signal regulator to regulate the photocurrent signal. First, the Au@NRs−CeO_2 octahedron competed with the photoelectric layer to absorb light energy owing to the broad absorption spectrum of Au NPs. Second, fast electron transfer occurred between Au NPs and NRs−CeO_2 through the SPR mechanism due to a Fermi level of Au NPs higher than that of the NRs−CeO_2 octahedron. The Au@NRs−CeO_2 octahedron consumed electron donors (AA) competing with the photoelectric layer. Third, the steric hindrance effect from the Au@NR−CeO_2 octahedron distinctly hindered the transfer process of electrons. The above three aspects cause a significant decrease in the photocurrent signal (Scheme 2B). As displayed in Scheme 2C, after the electrode incubation with a mixture of 4-CN and H_2O_2, the Au@NRs−CeO_2 octahedron could act as a peroxidase mimic to efficiently catalyze the formation of

Scheme 2. Mechanism of the Multiple Signal Amplification PEC Biosensor

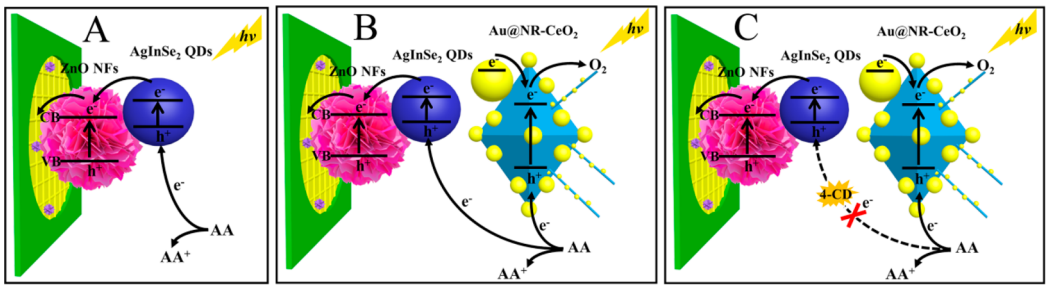

https://dx.doi.org/10.1021/acs.analchem.0c00231
Anal. Chem. XXXX, XXX, XXX−XXX

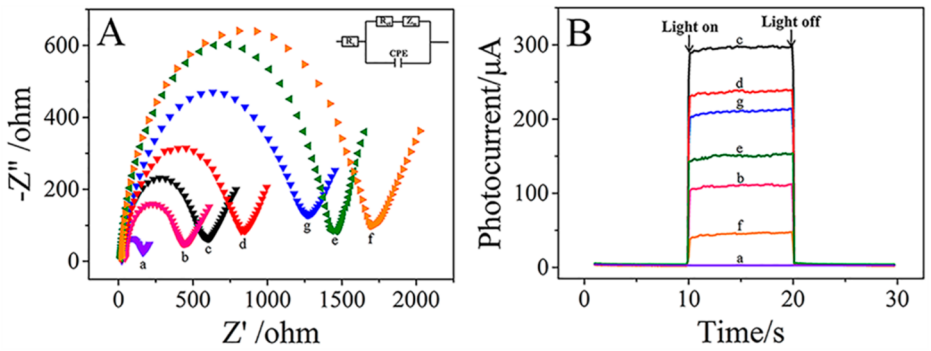

Figure 3. (A) EIS in 5 mM $[Fe(CN)_6]^{3-/4-}$ solution containing 0.1 M KCl and (B) photocurrent responses in PBS solution (pH 7.4) containing 0.1 M AA of (a) Au−PWE, (b) ZnO NFs/Au−PWE, and (c) $AgInSe_2$ QDs/ZnO NFs/Au−PWE (d) after CP immobilization and MCH blocking, (e) after Au@NRs−CeO_2−aDNA immobilization, (f) after incubation with 10 mM 4-CN and 1 mM H_2O_2, and then (g) further incubation with t-DNA.

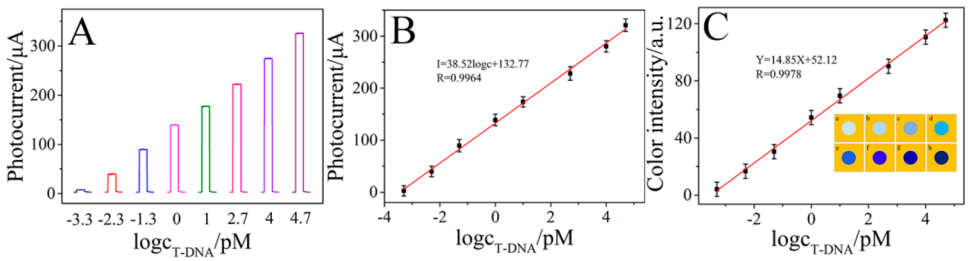

Figure 4. (A) Photocurrent responses of the PEC biosensor incubated with various concentrations of t-DNA. Calibration curves of (B) PEC responses and (C) color intensity versus logarithm of t-DNA.

MECP on the surface of the photoelectric layer, which further hindered the transfer of electrons and decreased the photocurrent signal again. When t-DNA was present, the Au@NRs−CeO_2 octahedron was released from the electrode surface due to the dissociation of the triple helix molecules, which caused a sharp increase in the photocurrent signal due to the disappearance of the quenching effect. Accordingly, a multiple signal amplification PEC biosensor was successfully built.

EIS and PEC Characterization of the Developed Biosensor. Electrochemical impedance spectroscopy (EIS) is a common method for monitoring the preparation process of the electrode surface of a PEC biosensor. The semicircular diameter measured by EIS reveals the interface charge transfer resistance (R_{et}) of the electrode. Figure 3A shows the impedance spectrum of the electrode involved in the different manufacturing steps, and the inset is a corresponding equivalent circuit. For Au−PWE, the impedance spectrum showed a relatively small semicircle (curve a), which proved that Au NPs had excellent electrical conductivity. However, after the step by step assembly of ZnO NFs and $AgInSe_2$ QDs, the R_{et} value increased sequentially due to the weak conductive property of the semiconductor (curve b and curve c). When the electrode ($AgInSe_2$ QDs/ZnO NFs/Au−PWE) was modified by the CP and MCH, the R_{et} value was visibly increased (curve d) on account of the nonconductivity of the nucleic acid and the organic molecule. After incubation with Au@NRs−CeO_2−aDNA, the steric hindrance effect from the Au@NRs−CeO_2 octahedron and the insulativity of the nucleic acid synergistically resulted in an increased R_{et} value again (curve e). Furthermore, after the electrode was incubated with a mixture of 4-CN and H_2O_2, the R_{et} value increased sharply (curve f). This is because the formation of insoluble benzo-4-chlorohexadienone (4-CD) precipitates further hindered the redox probe entering the electrode surface. When the t-DNA was present, the disassembly of the triple helix molecules kept Au@NRs−CeO_2−aDNA away from the electrode surface and eliminated the quenching effect, resulting in an appropriate decrease in the R_{et} value (curve g). The EIS results suggested that the designed PEC biosensor was successfully fabricated.

The characteristic of photocurrent response further verified the feasibility of the designed PEC biosensor. As shown in Figure 3B, the Au−PWE exhibited almost no photocurrent response (curve a). After ZnO NF modification, the photocurrent response was appropriately increased due to the excellent photoelectric activity of the ZnO NFs (curve b). When the electrode was further modified by the $AgInSe_2$ QDs, the photocurrent response significantly increased (curve c), which was attributed the absorption of near-infrared wavelength light by the $AgInSe_2$ QDs. However, after CP and MCH were immobilized, the photocurrent response decreased (curve d), which might be attributed to the fact that DNA and organic molecules hindered the transfer of electrons. After Au@NRs−CeO_2−aDNA was introduced into the electrode, the photocurrent output was further reduced (curve e). The reasons may be as follows: (1) the steric hindrance effect from the Au@NRs−CeO_2 octahedron impeded the transfer of electrons, (2) the Au@NRs−CeO_2 octahedron competitive consumption of electron donors (AA) and photon energy with the photoelectric layer. When t-DNA was not present, the photocurrent response obviously decreased after the electrode was incubated with 10 mM 4-CN and 1 mM H_2O_2, suggesting that the MECP further inhibited electron transfer (curve f). Subsequently, the photocurrent response significantly increased (curve g) when the electrode was incubated with t-DNA, and the results were consistent with EIS (Figure 3A, curve g). Accordingly, photocurrent response characterization demon-

https://dx.doi.org/10.1021/acs.analchem.0c00231
Anal. Chem. XXXX, XXX, XXX−XXX

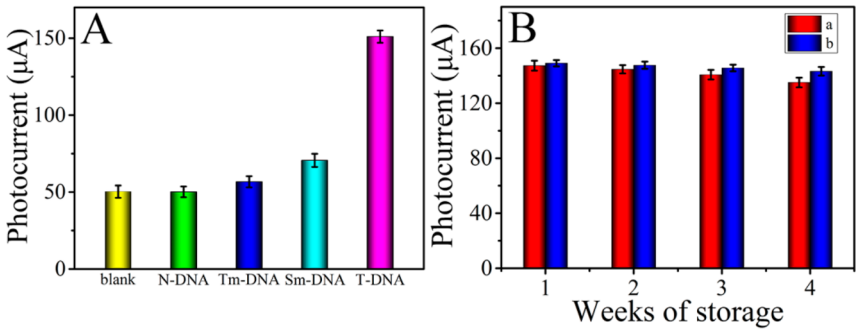

Figure 5. (A) Photocurrent responses of the PEC biosensor with different sequences of t-DNA (20 μL, 1 pM): (a) Blank, (b) N-DNA, (c) Tm-DNA, (d) Sm-DNA, (e) t-DNA. The error bars show the standard deviation of five independent experiments. (B) The stability of the proposed PEC biosensor at room temperature (a) and in the freezer (b).

strated that the multifunctional signal amplification strategy of the PEC biosensor was achieved.

PEC Detection of t-DNA. The t-DNA detection was based upon the disappearance of the quenching effects, and the photocurrent response of the biosensor was directly associated with the concentration of t-DNA. Figure 4A presents the photocurrent responses measured at different concentrations of t-DNA. As the concentration of t-DNA increased, more of the Au@NRs−CeO_2 octahedrons left the electrode surface and made the quenching effect disappear, leading to an increased photocurrent response. As displayed in Figure 4B, the photocurrent response linearly increased with an increasing logarithm of t-DNA concentration in the range from 0.5 fM to 50 nM. The regression equation was I = 38.52 log $c_{T\text{-}DNA}$ + 132.77 (R = 0.9964), and the limit of detection was estimated to be 0.28 fM at a signal-to-noise ratio of 3, which exhibited a wider linear range and lower detection limit than that of other work (Table S2). In addition, colorimetric analysis was used for visual detection of t-DNA. Because the chromogenic reactions could be catalyzed via the released Au@NRs−CeO_2 octahedron, the visualized detection could be achieved by measuring color intensity. As shown in Figure 4C, with the concentration of t-DNA increasing, the color of the colorimetric area of the colorimetric tab changes from colorless to blue. Moreover, a linear relationship was obtained between the color intensity and the logarithm of t-DNA concentration. The visual detection could be applied as a reference to initially judge the feasibility of the work.

Reproducibility, Selectivity, and Stability of the Biosensor. The reproducibility of the designed PEC biosensor was assessed via measuring five independently manufactured biosensors. The photocurrent responses offered a relative standard deviation (RSD) of 4.5% for 1 pM t-DNA, which confirmed a satisfactory precision and reproducibility of the biosensor.

To demonstrate the selectivity of the PEC biosensor toward t-DNA, under the same experimental conditions, experiments were carried out by analyzing the photocurrent responses of the PEC biosensor after hybridization with different DNA sequences: t-DNA, three-base mismatched DNA (Tm-DNA), single-base mismatched DNA (Sm-DNA), and noncomplementary DNA (N-DNA). As shown in Figure 5A, compared with the photocurrent response of the blank test, the N-DNA was almost identical but the t-DNA was significantly increased. For Tm-DNA and Sm-DNA, although the photocurrent responses were also increased, they were much lower than that of t-DNA. The results demonstrated that the proposed PEC biosensor was highly selective. To investigate the stability of this PEC biosensor, the developed biosensors were stored separately at room temperature (25 °C) and in a refrigerator (4 °C) and measured at intervals of 1 week. Figure 5B revealed that the obtained biosensor maintained a high photocurrent response regardless of whether it was stored at room temperature or in the freezer, suggesting a good long-term stability of the biosensor.

CONCLUSIONS

In summary, a multiple signal amplification PEC biosensor was successfully developed for ultrasensitive and visual determination of nucleic acids. $AgInSe_2$ QDs and a Au@NRs−CeO_2 octahedron were synthesized and used as the signal amplifier to improve the sensitivity of the biosensor. $AgInSe_2$, as a low-toxicity quantum dot, not only was used as a sensitizer for ZnO NFs to dramatically enhance the photocurrent signal but also provided a perfect application prospect in the construction of biosensors. The Au@NRs−CeO_2 octahedron acted as a multifunctional signal regulator. On the one hand, it could quench the photocurrent signal of the photoelectric layer due to the competitive consumption of electron donor and exciting light. On the other hand, it could also effectively catalyze the production of precipitation to hinder the transfer of electrons. In addition, the steric hindrance effect from the Au@NRs−CeO_2 octahedron further decreased the photocurrent signal of the biosensor. When t-DNA was present, the Au@NRs−CeO_2 octahedron left the electrode surface and flowed into the colorimetric area of the lab-on-paper device, which could further catalyze the occurrence of the color reaction to achieve a visual detection of t-DNA. Benefitting from the multiple signal amplification strategy and the low background signal for PEC detection, the proposed PEC biosensor showed perfect specificity, persuasive reproducibility, and satisfactory stability.

ASSOCIATED CONTENT

Supporting Information

The Supporting Information is available free of charge at https://pubs.acs.org/doi/10.1021/acs.analchem.0c00231.

Materials and reagents, design of the lab-on-paper analytical device, synthesis of 3D ZnO NFs, synthesis of GSH-stabilized $AgInSe_2$ QDs and preliminary application in human serum samples for nucleic acids (PDF)

https://dx.doi.org/10.1021/acs.analchem.0c00231
Anal. Chem. XXXX, XXX, XXX−XXX

AUTHOR INFORMATION

Corresponding Authors

Yunqing Liu − *Collaborative Innovation Center of Technology and Equipment for Biological Diagnosis and Therapy in Universities of Shandong, Institute for Advanced Interdisciplinary Research, University of Jinan, Jinan 250022, P.R. China*; Email: chm_liuyq@mail.ujn.edu.cn

Shenguang Ge − *Collaborative Innovation Center of Technology and Equipment for Biological Diagnosis and Therapy in Universities of Shandong, Institute for Advanced Interdisciplinary Research, University of Jinan, Jinan 250022, P.R. China*; orcid.org/0000-0002-0537-6491; Email: chm_gesg@163.com

Authors

Shaopeng Wang − *Collaborative Innovation Center of Technology and Equipment for Biological Diagnosis and Therapy in Universities of Shandong, Institute for Advanced Interdisciplinary Research, University of Jinan, Jinan 250022, P.R. China*

Fangfang Wang − *Collaborative Innovation Center of Technology and Equipment for Biological Diagnosis and Therapy in Universities of Shandong, Institute for Advanced Interdisciplinary Research, University of Jinan, Jinan 250022, P.R. China*

Cuiping Fu − *Collaborative Innovation Center of Technology and Equipment for Biological Diagnosis and Therapy in Universities of Shandong, Institute for Advanced Interdisciplinary Research, University of Jinan, Jinan 250022, P.R. China*

Yina Sun − *Collaborative Innovation Center of Technology and Equipment for Biological Diagnosis and Therapy in Universities of Shandong, Institute for Advanced Interdisciplinary Research, University of Jinan, Jinan 250022, P.R. China*

Jinge Zhao − *Collaborative Innovation Center of Technology and Equipment for Biological Diagnosis and Therapy in Universities of Shandong, Institute for Advanced Interdisciplinary Research, University of Jinan, Jinan 250022, P.R. China*

Na Li − *Collaborative Innovation Center for Green Chemical Manufacturing and Accurate Detection, School of Chemistry and Chemical Engineering, University of Jinan, Jinan 250022, P.R. China*

Jinghua Yu − *Collaborative Innovation Center for Green Chemical Manufacturing and Accurate Detection, School of Chemistry and Chemical Engineering, University of Jinan, Jinan 250022, P.R. China*; orcid.org/0000-0001-5043-0322

Complete contact information is available at: https://pubs.acs.org/10.1021/acs.analchem.0c00231

Author Contributions

[#]These authors contributed equally to this work.

Notes

The authors declare no competing financial interest.

ACKNOWLEDGMENTS

This work was supported by the National Natural Science Foundation of China (21775055, 21874055), a project of Shandong Province Higher Educational Youth Innovation Science and Technology Program (2019KJC016), The Project of "20 items of University" of Jinan (2018GXRC001), and The Taishan Scholars program and the Case-by-Case Project for Top Outstanding Talents of Jinan.

REFERENCES

(1) Hu, M.; Yang, H.; Li, Z.; Zhang, L.; Zhu, P.; Yan, M.; Yu, J. *Biosens. Bioelectron.* **2020**, *147*, 111786.

(2) Yue, Z.; Lisdat, F.; Parak, W. J.; Hickey, S. G.; Tu, L.; Sabir, N.; Dorfs, D.; Bigall, N. C. Quantum-dot-based photoelectrochemical sensors for chemical and biological detection. *ACS Appl. Mater. Interfaces* **2013**, *5* (8), 2800

(3) Yan, P.; Jiang, D.; Tian, Y.; Xu, L.; Qian, J.; Li, H.; Xia, J.; Li, H. *Biosens. Bioelectron.* **2018**, *111*, 74−81.

(4) Zhang, N.; Ruan, Y. F.; Zhang, L. B.; Zhao, W. W.; Xu, J. J.; Chen, H. Y. *Anal. Chem.* **2018**, *90* (3), 2341−2347.

(5) Zhao, J.; Wang, S.; Zhang, S.; Zhao, P.; Wang, J.; Yan, M.; Ge, S.; Yu, J. *Biosens. Bioelectron.* **2020**, *150*, 111958.

(6) Wang, S.; Zhao, J.; Zhang, Y.; Yan, M.; Zhang, L.; Ge, S.; Yu, J. *Biosens. Bioelectron.* **2019**, *139*, 111325.

(7) Zhao, W.-W.; Xu, J.-J.; Chen, H.-Y. *Anal. Chem.* **2018**, *90* (1), 615−627.

(8) Yang, R.; Yan, X.; Li, Y.; Zhang, X.; Chen, J. *ACS Appl. Mater. Interfaces* **2017**, *9* (49), 42482−42491.

(9) Shu, J.; Qiu, Z.; Lv, S.; Zhang, K.; Tang, D. *Anal. Chem.* **2018**, *90* (4), 2425−2429.

(10) Yang, R.; Zou, K.; Li, Y.; Meng, L.; Zhang, X.; Chen, J. *Anal. Chem.* **2018**, *90* (15), 9480−9486.

(11) Shu, J.; Tang, D. *Anal. Chem.* **2020**, *92* (1), 363−377.

(12) Yang, H.; Zhang, Y.; Zhang, L.; Cui, K.; Ge, S.; Huang, J.; Yu, J. *Anal. Chem.* **2018**, *90* (12), 7212−7220.

(13) Kong, Q.; Cui, K.; Zhang, L.; Wang, Y.; Sun, J.; Ge, S.; Zhang, Y.; Yu, J. *Anal. Chem.* **2018**, *90* (19), 11297−11304.

(14) Cao, C.; Xie, X.; Zeng, Y.; Shi, S.; Wang, G.; Yang, L.; Wang, C.-Z.; Lin, S. *Nano Energy* **2019**, *61*, 550−558.

(15) Shi, X. M.; Fan, G. C.; Shen, Q.; Zhu, J. J. *ACS Appl. Mater. Interfaces* **2016**, *8* (51), 35091−35098.

(16) Hou, T.; Zhang, L.; Sun, X.; Li, F. *Biosens. Bioelectron.* **2016**, *75*, 359−64.

(17) Li, M.; Liang, W.; Yuan, R.; Chai, Y. *ACS Appl. Mater. Interfaces* **2019**, *11* (12), 11834−11840.

(18) Zhang, Y.; Xu, R.; Kang, Q.; Zhang, Y.; Wei, Q.; Wang, Y.; Ju, H. *ACS Appl. Mater. Interfaces* **2018**, *10* (37), 31080−31087.

(19) Li, P.-N.; Ghule, A. V.; Chang, J.-Y. *J. Power Sources* **2017**, *354*, 100−107.

(20) Speranskaya, E. S.; Beloglazova, N. V.; Abe, S.; Aubert, T.; Smet, P. F.; Poelman, D.; Goryacheva, I. Y.; De Saeger, S.; Hens, Z. *Langmuir* **2014**, *30* (25), 7567−75.

(21) Kolny-Olesiak, J.; Weller, H. *ACS Appl. Mater. Interfaces* **2013**, *5* (23), 12221−37.

(22) Zhong, H.; Bai, Z.; Zou, B. *J. Phys. Chem. Lett.* **2012**, *3* (21), 3167−75.

(23) Fan, F.-J.; Wu, L.; Yu, S.-H. *Energy Environ. Sci.* **2014**, *7* (1), 190−208.

(24) Pinchetti, V.; Lorenzon, M.; McDaniel, H.; Lorenzi, R.; Meinardi, F.; Klimov, V. I.; Brovelli, S. *Nano Lett.* **2017**, *17* (7), 4508−4517.

(25) Jacob, R.; Okram, G. S.; Naduvath, J.; Mallick, S.; Philip, R. R. *J. Phys. Chem. C* **2015**, *119* (10), 5727−5733.

(26) Zhu, Y.; Liu, Y.; Wood, M.; Koocher, N. Z.; Liu, Y.; Liu, L.; Hu, T.; Rondinelli, J. M.; Hong, J.; Snyder, G. J.; Xu, W. *Chem. Mater.* **2019**, *31* (19), 8182−8190.

(27) Zhang, L.; Shi, X. M.; Xu, Y. T.; Fan, G. C.; Liang, Y. Y.; Wang, C.; Zhao, W. W. *Anal. Chem.* **2019**, *91* (10), 6403−6407.

(28) Li, M. J.; Zheng, Y. N.; Liang, W. B.; Yuan, R.; Chai, Y. Q. *ACS Appl. Mater. Interfaces* **2017**, *9* (48), 42111−42120.

(29) Mei, L.-P.; Jiang, X.-Y.; Yu, X.-D.; Zhao, W.-W.; Xu, J.-J.; Chen, H.-Y. *Anal. Chem.* **2018**, *90* (4), 2749−2755.

(30) Lin, Y.; Zhou, Q.; Tang, D.; Niessner, R.; Knopp, D. *Anal. Chem.* **2017**, *89* (10), 5637−5645.

https://dx.doi.org/10.1021/acs.analchem.0c00231
Anal. Chem. XXXX, XXX, XXX−XXX

(31) Zhuang, J.; Lai, W.; Xu, M.; Zhou, Q.; Tang, D. *ACS Appl. Mater. Interfaces* **2015**, *7* (15), 8330−8.
(32) Gong, L.; Dai, H.; Zhang, S.; Lin, Y. *Anal. Chem.* **2016**, *88* (11), 5775−82.
(33) Zhao, W. W.; Ma, Z. Y.; Yu, P. P.; Dong, X. Y.; Xu, J. J.; Chen, H. Y. *Anal. Chem.* **2012**, *84* (2), 917−23.
(34) Zheng, T.; Zhang, Q.; Feng, S.; Zhu, J. J.; Wang, Q.; Wang, H. *J. Am. Chem. Soc.* **2014**, *136* (6), 2288−91.
(35) Lin, Y.; Wu, L.; Huang, Y.; Ren, J.; Qu, X. *Chem. Sci.* **2015**, *6* (2), 1272−1276.
(36) Cui, L.; Hu, J.; Wang, M.; Diao, X. K.; Li, C. C.; Zhang, C. Y. *Anal. Chem.* **2018**, *90* (19), 11478−11485.
(37) Zeng, M.; Li, Y.; Mao, M.; Bai, J.; Ren, L.; Zhao, X. *ACS Catal.* **2015**, *5* (6), 3278−3286.
(38) Tao, L.; Shi, Y.; Huang, Y.-C.; Chen, R.; Zhang, Y.; Huo, J.; Zou, Y.; Yu, G.; Luo, J.; Dong, C.-L.; Wang, S. *Nano Energy* **2018**, *53*, 604−612.
(39) Zhao, H.; Dong, Y.; Jiang, P.; Wang, G.; Zhang, J. *ACS Appl. Mater. Interfaces* **2015**, *7* (12), 6451−61.
(40) Dong, Y. X.; Cao, J. T.; Liu, Y. M.; Ma, S. H. *Biosens. Bioelectron.* **2017**, *91*, 246−252.
(41) Li, M.; Cushing, S. K.; Wang, Q.; Shi, X.; Hornak, L. A.; Hong, Z.; Wu, N. *J. Phys. Chem. Lett.* **2011**, *2* (17), 2125−2129.
(42) Sztandera, K.; Gorzkiewicz, M.; Klajnert-Maculewicz, B. *Mol. Pharmaceutics* **2019**, *16* (1), 1−23.
(43) Zhu, J.; Huo, X.; Liu, X.; Ju, H. *ACS Appl. Mater. Interfaces* **2016**, *8* (1), 341−9.
(44) Li, C.; Sun, Y.; Djerdj, I.; Voepel, P.; Sack, C.-C.; Weller, T.; Ellinghaus, R.; Sann, J.; Guo, Y.; Smarsly, B. M.; Over, H. *ACS Catal.* **2017**, *7* (10), 6453−6463.
(45) Yan, J.; Yan, M.; Ge, L.; Ge, S.; Yu, J. *Sens. Actuators, B* **2014**, *193*, 247−254.

https://dx.doi.org/10.1021/acs.analchem.0c00231
Anal. Chem. XXXX, XXX, XXX−XXX